

---

# Effect of Mechanically Simulated Diaphragmatic Respiratory Motion on Myocardial SPECT Processed With and Without Attenuation Correction

Alexander G. Pitman, BMedSci, MBBS<sup>1</sup>; Victor Kalff, BMedSci, MBBS<sup>1</sup>; Bruce Van Every, BAppSci<sup>1</sup>; Borghild Risa, BAppSci<sup>1</sup>; Leighton R. Barnden, PhD<sup>2</sup>; and Michael J. Kelly, MBBS<sup>1</sup>

<sup>1</sup>Department of Nuclear Medicine, The Alfred Hospital, Prahran, Victoria, Australia; and <sup>2</sup>Department of Nuclear Medicine, The Queen Elizabeth Hospital, Woodville, South Australia, Australia

---

The goal of this study was to assess the effect of diaphragmatic respiratory motion on inferior wall cold artifact in myocardial SPECT and to assess the ability of attenuation correction (AC) to correct for this artifact in the presence of diaphragmatic motion. **Methods:** We used an anthropomorphic phantom with ventricular wall activity, variable ventricular caudal tilt, attenuating liver and spleen cold inserts, and variable vertical (diaphragmatic) motion amplitude and pattern. Cardiac SPECT images were acquired on a gamma camera with dual scanning transmission line sources and commercially available AC software (with scatter correction and iterative reconstruction). The acquired data were processed either using filtered backprojection or with the AC software. The resulting myocardial activity maps were processed with polar plots and with standardized inferior-to-anterior and anterior-to-lateral wall ratios. **Results:** Subdiaphragmatic attenuation reduces inferior wall counts and this component of inferior wall artifact is fully corrected by AC relative to anterior wall counts both with and without diaphragmatic respiratory motion. In the phantom, diaphragmatic motion artifact manifests as reduction in relative count density in both the anterior wall and the inferior wall relative to the lateral wall, which is not corrected by AC. This artifact becomes more marked with increasing respiratory amplitude and its symmetry depends on the pattern of diaphragmatic motion. **Conclusion:** Images with AC acquired at small respiratory amplitudes (~2 cm) in the phantom resemble images with AC found in published normal patient databases. These results support a clinical need for respiratory gating of myocardial SPECT images.

**Key Words:** respiratory motion artifact; diaphragmatic motion artifact; myocardial SPECT; inferior wall artifact; attenuation correction

**J Nucl Med 2002; 43:1259–1267**

---

**I**nferior wall artifact is a well-described empiric entity in myocardial perfusion studies. It is known by many synonyms, including diaphragmatic artifact, inferior wall attenuation artifact, liver artifact, and others (1). The usual appearance on myocardial SPECT studies is of a “cool” or “cold” inferior wall in the known absence of true inferior wall hypoperfusion. This is in effect a reduction in collected inferior wall counts not due to true reduction in inferior wall myocardial radioactivity concentration.

This artifact is most often attributed to subdiaphragmatic attenuation, and accordingly significant efforts have been directed at eliminating this artifact by attenuation correction (AC) using measured attenuation maps. Even though these efforts have been highly successful in phantom experiments, variable clinical acceptance has been achieved (2), and the use of electrocardiographically (ECG) gated SPECT to distinguish between infarct and artifact (3) has become widespread. ECG gating suggests that a fixed defect is an attenuation artifact if the involved myocardium contracts and thickens and that it is an infarct if it does not. Several studies of AC have identified pertinent physical issues such as the need for scatter correction (4,5) and the effect of depth-dependent blur (6,7). Further, the need for adequate quality control, adequate counting statistics, elimination of downscatter during transmission, and iterative reconstruction in acquired attenuation maps are all potential factors that influence the clinical reliability of this technique (8–10).

An alternative explanation for some of the variability in patient results may be related to respiratory motion, which has not usually been simulated in phantom experiments, even though it has been the subject of much preliminary work in the PET–CT fusion area (11,12). Therefore, we chose to use an anthropomorphic phantom to study this factor, as has recently been advocated (13).

---

Received Sep. 4, 2001; revision accepted Apr. 25, 2002.

For correspondence or reprints contact: Alexander G. Pitman, BMedSci, MBBS, P.O. Box 75, Parkville, Victoria 3052, Australia.  
Email: agpitman@unimelb.edu.au.

This study examines the contribution of diaphragmatic respiratory motion to the inferior wall cold artifact on myocardial SPECT images (i.e., diaphragmatic motion artifact). Specifically, it assesses the effect of respiratory amplitude and diaphragmatic motion pattern on myocardial SPECT images. It then examines the ability of one specific implementation of commercially available AC to correct inferior wall cold artifact in the presence of diaphragmatic motion as well as in its absence.

## MATERIALS AND METHODS

### Phantom Construction

The anthropomorphic phantom (Figs. 1 and 2A) comprised an ovoid acrylic cylinder (tub) (Fig. 1, no. 1) of such size and thickness as to mimic a human chest wall. The tub represented the combined attenuation produced by the ribs or intercostal muscle and the enveloping soft tissues. A cardiac insert (Data Spectrum, Chapel Hill, NC) (Fig. 1, no. 2) was held at 45° left anterior oblique in the axial plane and could be rotated to 0°, 15°, 30°, and 45° caudal angulation in the craniocaudal plane. The 0° setting was at strictly 0° caudal angulation (the long axis of the ventricle was strictly perpendicular to the camera detector face in the craniocaudal plane) to ensure strict geometric symmetry of the anterior and inferior walls and remove any potential effects of self-attenuation. The cardiac insert consisted of a typical left ventricle-size chamber surrounded by a hollow myocardial jacket. The apex-to-base length of the entire heart was 85 mm, and outside diameter was 60 mm. The left ventricular cavity was 35 mm in diameter and had 60-mL capacity. It was filled with saline. The myocardial jacket had 118-mL capacity and was filled either with  $^{201}\text{Tl}$  or  $^{99\text{m}}\text{Tc}$  (simulating methoxyisobutylisonitrile [MIBI] activity) depending on the experiment. A 3-mm acrylic diaphragm (Fig. 1, no. 3) could be placed immediately below the cardiac insert to create an abdominal compartment. Saline bags (Fig. 1, no. 4) could be packed under the diaphragm to simulate liver and spleen. The diaphragm ensured that the saline bags remained tightly packed in the abdominal compartment. The ventricle was surrounded by only air in the

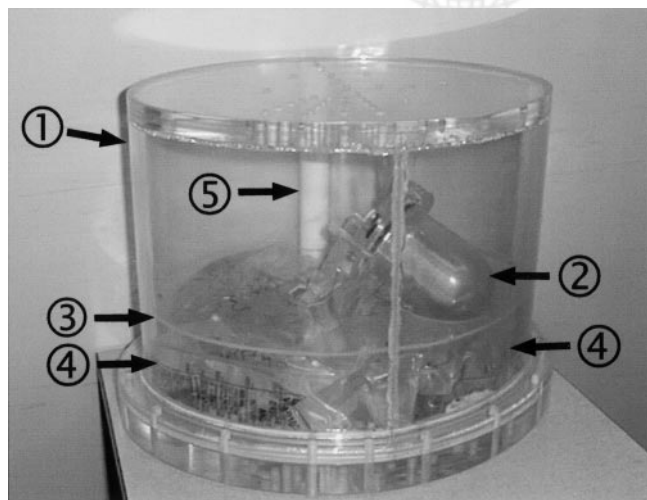


**FIGURE 1.** Photograph of phantom shows its components: 1, acrylic tub; 2, cardiac insert; 3, acrylic diaphragm; 4, saline bags; 5, Teflon (DuPont, Wilmington, DE) spine.

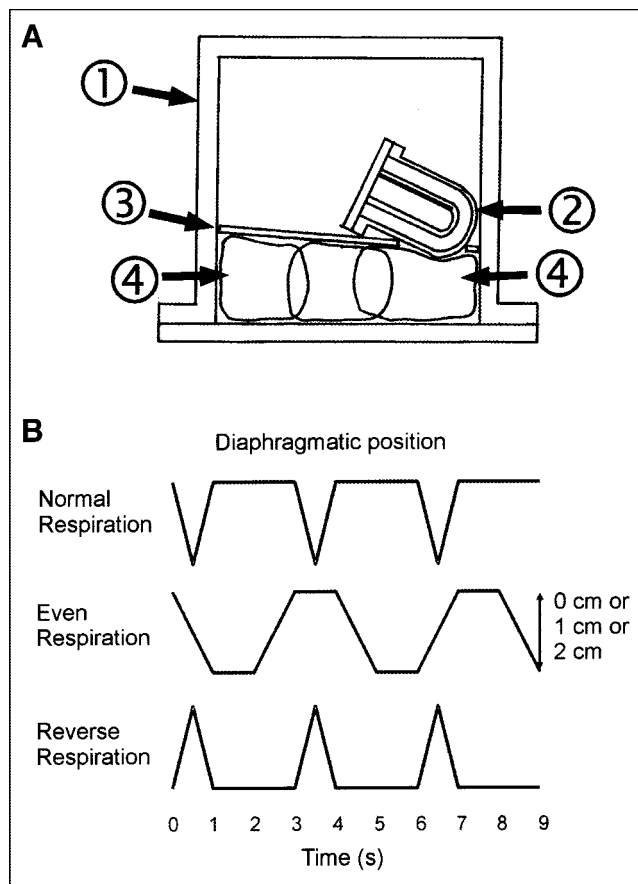


**FIGURE 2.** (A) Schematic diagram of midcoronal section through phantom shows relationship between saline bags and cardiac insert. Components of phantom are numbered same as in Figure 1. (B) Respiratory patterns used for phantom experiments. x-axis: time (s); y-axis: position of diaphragm. Cranial is up.

chest compartment (pilot acquisitions with lung inserts produced the same images as images without lung inserts; therefore, the simpler setup was used). When the ventricle was caudally angulated, its apex rested directly against the saline bags within the apical cutout of the diaphragm, and the right hemidiaphragm rose above the apex. This arrangement was anatomically correct. A Teflon (DuPont, Wilmington, DE) column (Fig. 1, no. 5) (spine) was located posteriorly in its anatomically correct position.

### Phantom Motion

A healthy adult male volunteer was used to confirm the physiologic range of diaphragmatic respiratory motion. He underwent fast supine MRI in quiet inspiration and quiet expiration. The right leaf of the diaphragm, left leaf of the diaphragm, and middiaphragmatic tendon were taken as references to calculate diaphragmatic excursion in quiet respiration.

To validate our choice of respiratory rates, we counted the respiratory rate in 10 male and 10 female patients while they were scanned after exercise (on average, 10 min after cessation of exercise).

In our model, we made the simplifying assumption that movement of the heart with respiration primarily follows the movement of the diaphragm. In the phantom, respiratory motion of the heart

with the diaphragm was simulated by motion of the entire phantom in the vertical (craniocaudal) direction (Fig. 2B). This approximation was used because phantom geometry allowed substitution of motion of the entire phantom for motion of the heart, diaphragm, and abdominal compartment within the phantom's shell. Smaller amplitude, more complex motions of the heart that occur with respiration (effect of chest wall expansion, change in heart shape, and so forth) were not modeled.

The phantom was moved on a purpose-built gantry (a specifically designed and constructed frame allowing craniocaudal phantom motion). The gantry was built of low-density polyvinyl chloride tubing to offer as little photon attenuation as possible. It was also placed posteriorly below the phantom and so intruded as little as possible on the right anterior oblique (RAO) to left posterior oblique (LPO) semicircular acquisition path. The gantry consisted of an inner rectangular frame (Fig. 3, no. 1) fixed to the camera bed and an outer sliding gantry (Fig. 3, no. 2) holding the phantom.

The phantom was moved on the gantry by hand, with a smooth motion from one end position to the other. Uniformity and reproducibility were achieved by strict timing using a seconds counter. The range of craniocaudal travel of the gantry either was 10, 20, or 30 mm (respiratory amplitude).

There was no phasic relationship between the acquisition protocol and the phantom's respiratory cycle, and there was no systematic emission–transmission misregistration. The step-and-shoot protocol involved emission scans of 40 s each, during which the phantom moved for approximately  $40/3 = 13.3$  respiratory cycles (for normal motion), and transmission scans of 10 s each, during which the phantom moved for approximately  $10/3 = 3.3$  cycles; in addition, respiratory cycles continued during the time taken by the camera to move to the next angular position. As a result of the respiratory cycles being considerably shorter than either the emission or the transmission scans, there was averaging of phantom projections (both emission and transmission) on the detector face during each step; this contributed to the motion artifact, but there was no synchrony between the respiratory cycle and the timing of the acquisition. Because both the emission and the transmission

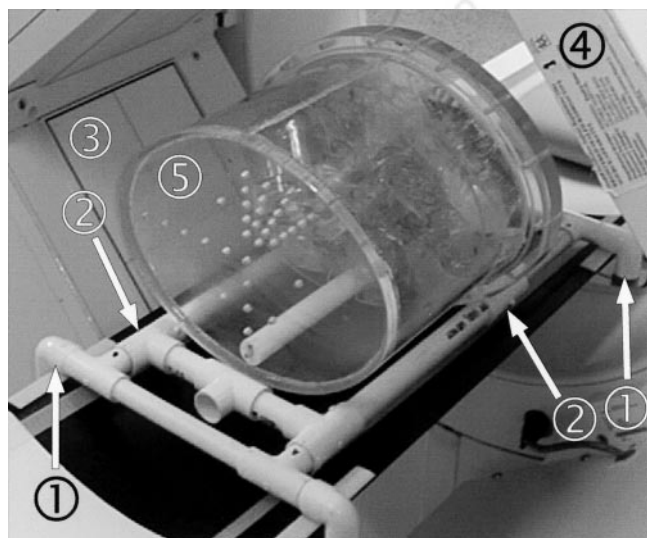


**FIGURE 3.** Photograph of gantry assembly on gamma-camera bed: 1, fixed frame; 2, sliding frame; 3, L-shaped detectors; 4, transmission source; 5, phantom (oriented supine, cranial to left). Push–pull handle has been removed for photography.

scans were blurred by the same amount, there was no emission–transmission misregistration.

With diaphragmatic motion, the cold attenuating spleen and liver moved into the position occupied previously by the myocardium, so that count averaging occurred between them and the myocardium.

In our experiments we acquired images of the immobile phantom and also examined 3 different patterns of diaphragmatic motion (Fig. 2B):

- Normal respiration was defined as inspiration and expiration over 1 s, followed by a 2-s expiratory pause. The respiratory rate was 20 breaths per minute, and the respiratory amplitude was 10, 20, or 30 mm.
- Reverse respiration was defined as expiration and inspiration over 1 s, followed by a 2-s inspiratory pause. The respiratory rate was 20 breaths per minute, and the respiratory amplitude was 10, 20, or 30 mm. Reverse respiration is analogous (although not fully identical) to respiration in severe chronic obstructive pulmonary disease or status asthmaticus, with a short inspiration and then a slower longer expiration.
- Even respiration was defined as inspiration over 1 s followed by a 1-s inspiratory pause, then expiration over 1 s followed by a 1-s expiratory pause. The respiratory rate was 15 breaths per minute, and the respiratory amplitude was 10, 20, or 30 mm. Even respiration is analogous to respiration during or shortly after exercise, when the respiratory pause decreases.

### Image Acquisition and Processing

The methodology was similar to that described by Prvulovich et al. (14) but with specific parameters as below. All tomographic (SPECT) images were acquired on an Optima NX gamma camera (General Electric Medical Systems, Milwaukee, WI). The camera has 2 perpendicular detectors (field of view,  $183 \times 337$  mm, fitted with low-energy, high-resolution collimators) in an L configuration. The acquisition protocol was  $90^\circ$  step and shoot, with 16 steps for each detector, using a  $64 \times 64$  matrix and 6-mm pixel size. Hence, a total of 32 angles were acquired and encompassed a semicircular orbit from RAO  $45^\circ$  to LPO  $45^\circ$ . At each step the emission image was acquired first over 40 s, followed by a transmission image over 10 s (interleaved emission/transmission acquisition). Moving  $^{153}\text{Gd}$  line sources (each with 2.7 GBq of activity at the time of the experiment) were used for transmission image acquisition.

The energy windows were as follows: for  $^{99\text{m}}\text{Tc}$ , 140 keV 20% wide, 0% offset; for  $^{201}\text{Tl}$ , 72 keV 20% wide, 0% offset; for  $^{153}\text{Gd}$  and cross-talk, 100 keV 20% wide, 0% offset; and for scatter, 60 keV 20% wide, 0% offset. An electronic transmission scan mask was used to help reduce the cross-talk from the emission scan (the 140-keV  $^{99\text{m}}\text{Tc}$  or the 167-keV  $^{201}\text{Tl}$  photons) into the transmission image (the 100-keV  $^{153}\text{Gd}$  window). The transmission scan mask width was 350 mm (i.e., the detector field of view) in the  $x$ -direction (line source direction) and 72 mm in the  $y$ -direction (scanning direction). Total acquisition time for the entire study was 13 min 20 s.

Representative images of attenuation maps acquired with and without motion are shown in Figure 4.

All collected data were processed using filtered backprojection (FBP) without any AC and using iterative reconstruction with scatter correction and AC.

Processing parameters for FBP were Butterworth filter (critical frequency, 0.31 cycle/cm; power factor, 7). Parameters for AC

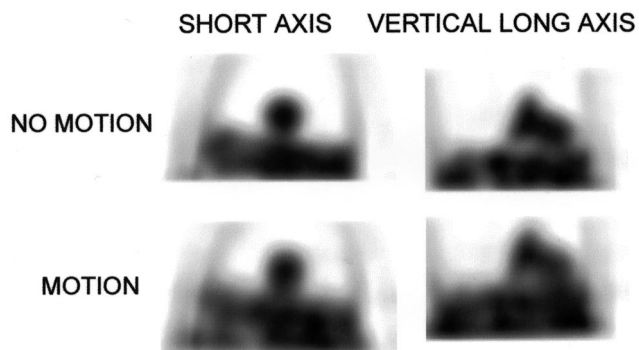


**FIGURE 4.** Four illustrative slices of transmission map for vertical short axis with no motion (top left) and with 2 cm of motion (bottom left) and for vertical long axis with no motion (top right) and with 2 cm of motion (bottom right). Heart was at 30° caudal angulation; cold liver and spleen inserts were present. Respiratory pattern was normal respiration.

were transmission: Hanning filter (critical frequency, 0.4 cycle/cm); iterative reconstruction: ordered subsets expectation maximization, 2 iterations; postemission filtering: Butterworth filter (critical frequency, 0.31 cycle/cm; power factor, 7).

The resulting SPECT ventricular activity map was presented for visual interpretation in a standard tomographic fashion (short-axis, vertical long-axis, and horizontal long-axis slices) and as a distance-weighted polar plot (giving an accurate depiction of defect position). The datasets were also analyzed quantitatively.

#### Quantitative Analysis

The myocardial activity map was divided into 8 short-axis doughnut sections, from base to apex. In each section, a  $12 \times 12$  mm box region of interest (ROI) was placed in the center of the anterior, inferior, and lateral walls and of the septum, and mean counts in each ROI were obtained. The 8 values for each wall were used to increase the statistical power of the analysis. The values from the lateral wall and the septum were averaged because the heart contained the left ventricle only and so was symmetric.

Wall activity ratios were calculated for each acquisition; because these were ratios and were normalized to the lateral wall or septum, meaningful comparison of different acquisitions was possible.

The inferior-to-anterior wall ratio was used to quantitate the inferior wall attenuation artifact. The anterior-to-lateral wall ratio was used to quantitate the diaphragmatic motion artifact, because the anterior wall was free of any attenuation from adjacent structures or from self-attenuation by the ventricle.

#### Specific Experiments

*Effect of Respiratory Pattern and Amplitude.* For this series of experiments the ventricle was set perpendicular to the detector face (i.e., 0° caudal angulation). The myocardial jacket contained 40 MBq  $^{99m}\text{Tc}$  (simulating physiologic amount of MIBI). No liver or spleen attenuators were used, and there was no diaphragmatic insert. The phantom either was immobile or had a respiratory amplitude of 10, 20, and 30 mm for each of the normal, even, and reverse respiratory patterns.

*Combination of Diaphragmatic Motion and Attenuation Artifacts.* In this series of experiments the myocardial jacket contained 4.5 MBq  $^{201}\text{Tl}$ . The phantom either was immobile or was moved

with normal respiration for an amplitude of 10 or 20 mm. The ventricle was caudally angulated at 15°, 30°, or 45°. The diaphragmatic insert and liver and spleen cold attenuators were used throughout.

#### RESULTS

In the healthy volunteer during quiet respiration, the extent of craniocaudal motion at the dome of the diaphragm was 20, 11, and 10 mm for the right leaf, central tendon, and left leaf, respectively. The greatest extent of craniocaudal motion was 28, 15, and 19 mm for the right leaf, central tendon, and left leaf, respectively, and lay posterior to the coronal plane of the dome. The minimal extent of motion was 0 mm at the attachment points of the diaphragm. The craniocaudal movement of the heart closely followed the movement of the diaphragm.

In the 20 patients whose respiratory rate was counted during scanning, the rate varied between 16 and 21 breaths per minute, with a mean respiratory rate of 18 breaths per minute.

#### Effect of Respiratory Pattern and Amplitude

Figure 5 shows the effect of pure diaphragmatic motion on the myocardial SPECT images. With the phantom stationary, the demonstrated activity is symmetric in all of the walls, and there is no perceptible difference between FBP and AC images. With motion, diaphragmatic motion artifact manifests itself as a reduction in perceived count density in both the anterior and the inferior walls. Diaphragmatic motion artifact is barely apparent with 10 mm of motion, is clearly visible with 20 mm of motion, and is gross with 30 mm of motion. Images processed with AC show no visible difference from the images processed with FBP, indicating that AC does not have any effect on diaphragmatic motion artifact.

The location of the worst artifact is dependent on the respiratory pattern. With the even pattern, the artifact in the anterior and the inferior wall is symmetric. With the normal pattern, the artifact is more severe in the inferior wall, and with the reverse pattern of respiration it is a mirror image of the normal pattern and is more severe in the anterior wall. This pattern-dependent asymmetry is invisible at 10 mm of motion, is clearly present at 20 mm, and is gross at 30 mm.

#### Combination of Diaphragmatic Motion and Attenuation Artifacts

Figure 6 shows the polar plots and midventricular vertical long-axis slices for 0, 10, and 20 mm of normal respiratory motion for both FBP and AC processing with the ventricle at 30° caudal angulation.

Figure 7A shows the inferior-to-anterior ratio as a function of respiratory amplitude. Figure 7B shows the anterior-to-lateral ratio as a function of respiratory amplitude for the 30° caudal ventricle.

Table 1 presents the inferior-to-anterior and anterior-to-lateral ratios in numeric form for 0, 10, and 20 mm of

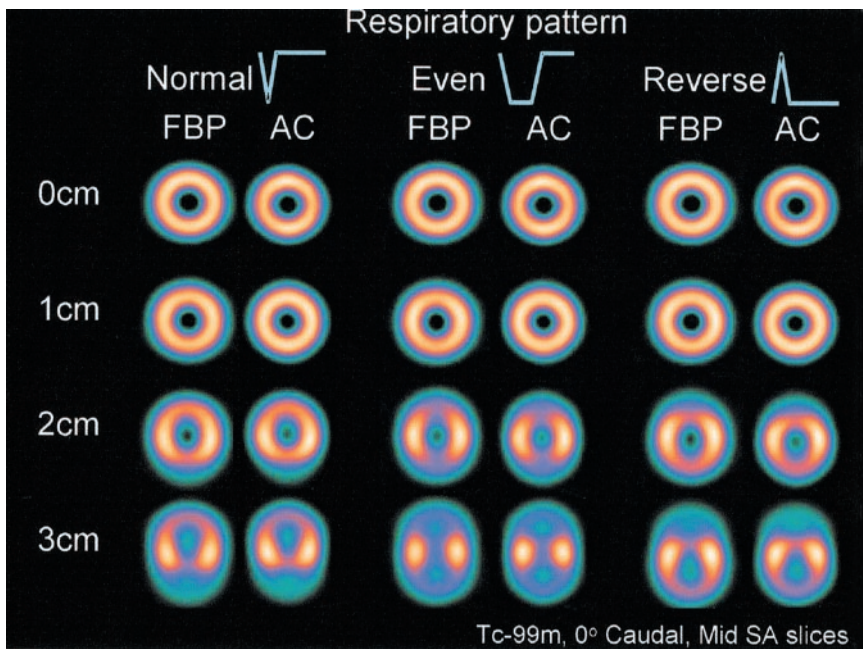


**FIGURE 5.** Demonstration of respiratory motion artifact and its dependence on respiratory pattern. For these experiments, myocardial inferior wall self-attenuation was avoided by positioning heart truly horizontally (perpendicular to face of detector), and no liver or spleen inserts were present. Myocardial insert contained 40 MBq <sup>99m</sup>Tc. Mid-short-axis (SA) slices are illustrated. Normal, Even, Reverse = respiratory pattern (see Fig. 2B); AC = measured transmission AC with iterative reconstruction and scatter correction; 0, 1, 2, and 3 cm = respiratory amplitude of phantom.

normal respiratory motion and 15°, 30°, and 45° of caudal angulation.

At 30° caudal angulation, in the immobile phantom and with FBP processing, the inferior wall activity is visibly reduced compared with that of the anterior wall. This is solely the effect of attenuation. AC effectively corrects this. With 20 mm of motion, the inferior wall cold artifact becomes more severe, and now there is also a reduction in the anterior wall activity (relative to the lateral wall). This is a manifestation of diaphragmatic motion artifact. Both the anterior and inferior wall activities are reduced comparably, so that the relationship of the inferior wall to the anterior wall is preserved. AC restores inferior wall activity to a

level similar to that of the anterior wall. However, it fails to restore either the anterior or the inferior wall activity toward the level of the lateral wall (Fig. 6).

The inferior-to-anterior ratio for FBP processing is reduced with no motion and does not change with respiratory amplitude. Application of AC either corrects or slightly overcorrects the inferior-to-anterior ratio (Fig. 7A). The anterior-to-lateral ratio for FBP processing is greatest with no motion and progressively decreases with increasing amplitude. AC does not make any difference to the anterior-to-lateral ratio (Fig. 7B).

Varying the ventricle caudal angulation has the following effect (Table 1). The inferior-to-anterior ratio decreases

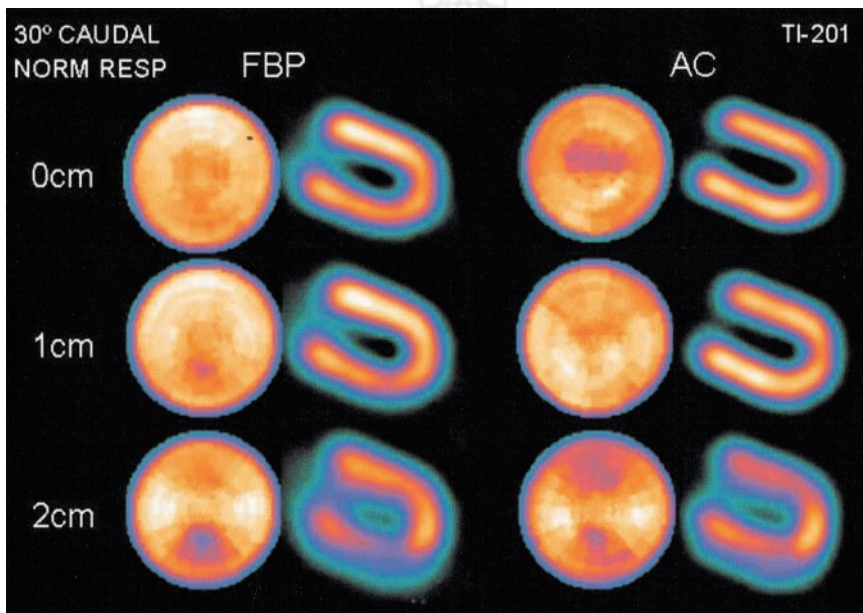


**FIGURE 6.** Interaction of attenuation artifact and respiratory motion artifact. Heart was at 30° caudal angulation; cold liver and spleen inserts were present. Myocardial insert contained 4.5 MBq <sup>201</sup>Tl. Respiratory pattern was normal respiration. Distance-weighted polar plots and midvertical long-axis slices are illustrated. Normal = respiratory pattern (see Fig. 2B); AC = measured transmission AC with iterative reconstruction and scatter correction; 0, 1, and 2 cm = respiratory amplitude of phantom.

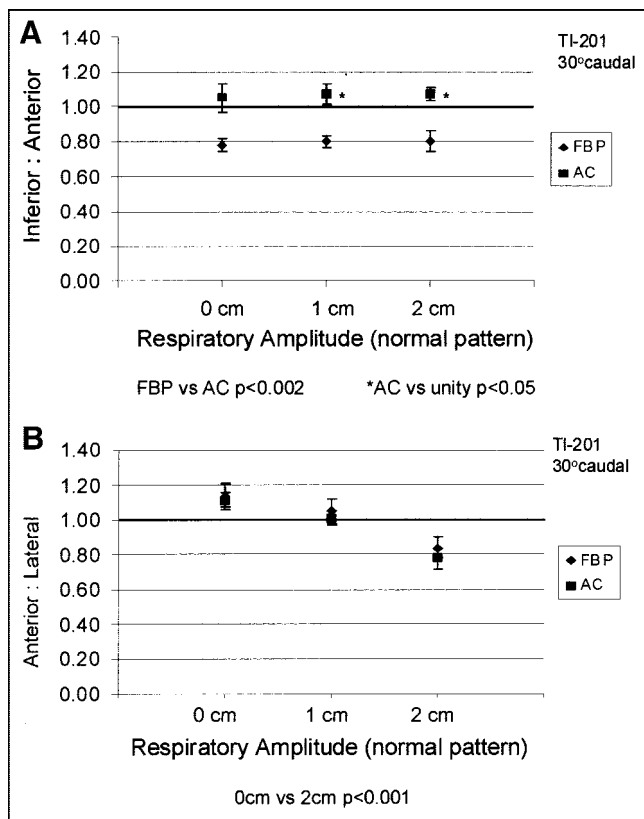


**FIGURE 7.** Representative graphs of inferior-to-anterior myocardial activity ratio (A) and anterior-to-lateral activity ratio (B) as function of respiratory amplitude. Heart was at 30° caudal angulation; cold liver and spleen inserts were present. Myocardial insert contained 4.5 MBq  $^{201}\text{Tl}$ . Respiratory pattern was normal respiration. FBP = FBP processing; AC = measured transmission AC with iterative reconstruction and scatter correction processing.

with progressive caudal angulation, whereas AC significantly corrects the inferior-to-anterior ratio for all caudal angles and respiratory amplitudes. At shallow caudal angles and greater respiratory amplitudes, AC tends to increasingly overcorrect the inferior wall activity. At all caudal angles, the anterior-to-lateral ratio significantly decreases as the respiratory amplitudes increase, whereas AC does not change the anterior-to-lateral ratio compared with FBP.

## DISCUSSION

These experiments have clearly shown that, in our model, diaphragmatic motion artifact is a contributor to the inferior wall cold artifact and is independent of inferior wall attenuation artifact.

In examining the contribution of respiratory motion to inferior wall artifact we chose to use a physical phantom rather than a computer phantom. In our opinion, physical phantoms are more valid than computer models, but they inevitably have limitations. We were unable, within practical limits, to model myocardial contraction and respiratory chest wall expansion with our physical phantom. Other

effects of respiratory motion on the size and shape of the heart affect both the emission data and the transmission map. Without denying that these motions also contribute to respiratory motion artifact, we chose to concentrate on the effect of isolated diaphragmatic motion. Motion of the left ventricle during the respiratory cycle closely follows motion of the diaphragm, as shown with MRI both by Holland et al. (15) and by us. This motion has greater amplitude than other motions associated with respiration and is the most clinically relevant. In our model we made the simplifying assumption that the heart moves in unison with the diaphragm. Because of the symmetric construction of our phantom, substitution of whole phantom motion for motion of the diaphragm, heart, liver, and spleen is practical and justifiable. Clearly, further patient-based studies will be required for those issues in respiratory motion artifact that cannot be addressed with a physical phantom.

In our study, diaphragmatic motion artifact manifests itself as a relative reduction in apparent count density that affects both the anterior wall and the inferior wall compared with the lateral wall and the septum. On polar plots it produces characteristic cool areas at the approximately 12 o'clock and 6 o'clock positions. The pattern of respiratory motion determines the antero-inferior dominance pattern of diaphragmatic motion artifact. With the normal pattern of respiration the inferior wall shows the greatest severity of artifact. Quantitative analysis of this diaphragmatic motion artifact and the mathematic basis for its causation and for its anterior-to-inferior asymmetry in the absence of any attenuation have been presented by us as an abstract (16).

As more experience has accumulated with AC, it has become clear that meticulous AC technique is necessary to produce optimal AC images. This includes the use of iterative reconstruction, scatter correction, depth-dependent correction, motion correction, and quality control for both the emission and the transmission datasets (8–10). Misalignment between the transmission and emission scans has also been shown to produce artifact (17), with as little as 1-pixel (7 mm) shift producing a 15% change of relative regional wall activity. Emission–transmission misregistration was not contributing to diaphragmatic motion artifact shown in our model. Gross patient motion has long been recognized as a cause of artifact (18–20). Correction for patient movement between acquisition frames has been shown to improve the accuracy of AC (7) and is strongly advised. However, no respiratory motion correction is currently applied during clinical AC image acquisition.

AC combined with scatter correction is widely used clinically and has had both unfavorable (21–23) and a larger proportion of favorable (7,22,24,25) reports. Ficaro et al. (24) constructed normal MIBI polar activity AC and non-AC maps for men ( $n = 10$ ) and women ( $n = 10$ ) with low likelihood of coronary artery disease. AC maps in these patients corrected the sex difference seen in the non-AC maps but showed a 10%–15% reduction in activity at the apex and a reduction in activity of the distal anterior wall.

**TABLE 1**  
Effect of Ventricle Caudal Angulation and Respiratory Amplitude on Inferior-to-Anterior and Anterior-to-Lateral Wall Ratios

201Tl wall ratio	Amplitude (cm)	Angle					
		15°		30°		45°	
		FBP	AC	FBP	AC	FBP	AC
Inferior-to-anterior*	0	0.97 ± 0.04 <sup>†</sup>	1.11 ± 0.07 <sup>†‡</sup>	0.78 ± 0.04	1.05 ± 0.08	0.72 ± 0.10	0.98 ± 0.13
	1	0.94 ± 0.04 <sup>†</sup>	1.11 ± 0.04 <sup>†‡</sup>	0.80 ± 0.03	1.07 ± 0.06 <sup>‡</sup>	0.75 ± 0.11	0.92 ± 0.12
	2	0.96 ± 0.07 <sup>†</sup>	1.22 ± 0.05 <sup>†‡</sup>	0.80 ± 0.06	1.07 ± 0.04 <sup>‡</sup>	0.69 ± 0.13	0.95 ± 0.16
Anterior-to-lateral <sup>§</sup>	0	1.00 ± 0.07 <sup>¶</sup>	1.10 ± 0.07 <sup>¶</sup>	1.14 ± 0.07 <sup>¶</sup>	1.11 ± 0.05 <sup>¶</sup>	1.05 ± 0.07 <sup>¶</sup>	1.05 ± 0.06 <sup>¶</sup>
	1	0.91 ± 0.08	0.88 ± 0.04	1.05 ± 0.07	1.01 ± 0.04	0.95 ± 0.07	0.92 ± 0.08
	2	0.75 ± 0.05	0.74 ± 0.03	0.84 ± 0.06	0.78 ± 0.06	0.88 ± 0.06	0.80 ± 0.08

\*All inferior-to-anterior FBP vs. AC pairs,  $P < 0.002$ .

<sup>†</sup>All inferior-to-anterior 15° vs. 45° pairs,  $P < 0.05$ .

<sup>‡</sup>Inferior-to-anterior AC vs. unity,  $P < 0.05$ .

<sup>§</sup>All anterior-to-lateral FBP vs. AC pairs,  $P =$  not significant.

<sup>¶</sup>All anterior-to-lateral 0-cm vs. 2-cm pairs,  $P < 0.001$ .

Data are expressed as mean ± 1 SD. Cold liver and spleen inserts were present. Respiratory pattern was normal respiration.

This was attributed to likely partial-volume effect. Similar findings are seen in the AC polar maps in other clinical studies, including the work of Gallowitsch et al. (25), Prvulovich et al. (14), Chouraqui et al. (26), and Kluge et al. (27). In all of these studies the investigators attributed such findings to similar causation. The pattern is also evident in more recent reports examining AC with depth correction (28).

All of these normal AC maps have a striking resemblance to the AC polar plots generated in our study with 30° ventricle caudal angulation, subdiaphragmatic cold attenuation, and 10–20 mm of respiratory motion (Fig. 6). It is possible that the mild reduction in anterior and inferior wall activity in the normal AC databases represents unmasking of respiratory blur with technically successful AC algorithms.

In the immobile phantom where diaphragmatic motion artifact is not superimposed, AC tends to overcorrect the inferior wall at shallow caudal angulations. A similar increase in inferior wall ratios beyond unity has been observed in patients (14,23). With superimposed motion, AC still corrects the inferior-to-anterior ratios, and its tendency to overcorrect these ratios beyond unity becomes more marked with increasing respiratory amplitude.

Because the mechanism of diaphragmatic motion artifact is not derived primarily from attenuation, it can be expected that AC will not have any significant effect on it. This was borne out experimentally. Although AC restores the inferior wall activity to the level of the anterior wall, it does not restore it to the level of the lateral wall and septum, and the residual inferior wall cold artifact largely represents diaphragmatic motion artifact. In a human the situation is more complex, with both cardiac shape and position changing even though cardiac movement with the diaphragm still has the greatest amplitude. The attenuation map will change

with respiratory motion as well, and this has implications for which AC methods may be compatible with respiratory motion correction (vide infra). A clinical study by Cho et al. (29) looked at the effect of respiratory gating during cardiac SPECT in healthy male volunteers. They found that respiratory gating led to improved inferior wall activity and that inferior wall activity in inspiration was statistically greater compared with that in expiration. Thus, the findings of our study are in agreement with their clinical findings.

Diaphragmatic motion artifact becomes progressively more marked with increasing respiratory excursion. It is just seen at 10-mm respiratory amplitude but is readily apparent at 20-mm respiratory amplitude. This is clinically relevant because the severity of diaphragmatic motion artifact may vary in the same individual between stress (deeper respiration) and rest (shallower respiration) acquisitions. The relative reduction in the anterior wall activity relative to that of the lateral wall (quantified in the anterior-to-lateral ratio) became progressively more marked with increasing respiratory amplitude and was the same for both FBP and AC.

At present, we are unsure how much cardiac contraction and cardiac motion with the diaphragm each contribute to the inferior wall cold artifact. Determination of the relative role of each will require clinical studies that can apply both ECG and respiratory gating.

Therefore, we recommend introduction and clinical use of respiratory gating for myocardial SPECT studies to eliminate diaphragmatic motion artifact. In the first instance, data acquisition during the end-expiratory pause or during breathholding is feasible, may be appropriate, and will incur only a relatively small time penalty. A recent MRI-based study (15) showed that diaphragmatic movement occurs even with breathholding, but the magnitude of cardiac displacement due to this is too small to significantly affect SPECT.

Respiratory gating at present is very much a proprietary technology and tends to be specific to the manufacturer. Cho et al. (29) used the gallbladder as a reference point in MIBI studies to respiratory gate list-mode acquisitions. Respiratory gating in MRI may use bellows (General Electric Medical Systems) or other mechanical or optomechanical technology. As list-mode acquisition becomes more feasible and navigator techniques become adapted from MRI to myocardial SPECT, it should become possible to perform respiratory and ECG gating (double gating) without any prolongation of acquisition time.

Respiratory gating should be applied equally to both the emission and the transmission data to avoid any misregistration artifact, which is likely to cause foci of artifactually elevated counts. It is conceivable that some of the inferior wall overcorrection in AC studies may in part be due to emission–transmission misregistration. If this hypothesis is proven, design of transmission sources and systems will need to be compatible with respiratory gating. Of the methods currently in use, the fanbeam source and the static array of line sources appear better suited to respiratory gating than the scanning line source.

Finally, diaphragmatic motion artifact is only one of many factors affecting myocardial perfusion SPECT. All of the currently available technical improvements described above should still be applied in myocardial SPECT studies together with respiratory gating to produce the best possible AC.

## CONCLUSION

In a physical phantom model examining the effect of cardiac movement with diaphragmatic respiratory motion on cardiac SPECT, diaphragmatic motion artifact manifests as a reduction in apparent count density in both the anterior wall and the inferior wall relative to that of the lateral wall and is independent of the presence of subdiaphragmatic attenuators. AC fails to correct this artifact, even though it successfully corrects the effects of attenuation. Diaphragmatic motion artifact becomes more marked with increasing respiratory amplitude and its symmetry depends on the pattern of diaphragmatic motion. Images acquired with AC at small respiratory amplitudes (~2 cm) in the phantom resemble images with AC seen in published normal patient databases, suggesting that diaphragmatic motion artifact contributes to inferior wall artifact in clinical patient studies. Clinical studies with respiratory as well as ECG gating (double gating) would be the next logical step in further determining the contribution of diaphragmatic respiratory motion to cardiac inferior wall artifact.

## ACKNOWLEDGMENTS

The authors thank Stephen Stuckey, MBBS, Director of MRI at The Alfred Hospital Melbourne, for his help with the MRI study of normal diaphragmatic motion. This work was presented in part at the 48th Annual Meeting of the

Society of Nuclear Medicine, Toronto, Ontario, Canada, June 23–27, 2001.

## REFERENCES

1. Elson SH, Clark WS, Williams BR. Is 'diaphragmatic' attenuation a misnomer? evaluation of the anatomic cause of 'diaphragmatic' attenuation in SPECT thallium scanning. *Int J Cardiol.* 1997;13:161–164.
2. Corbett JR, Ficaro EP. Clinical review of attenuation corrected cardiac SPECT. *J Nucl Cardiol.* 1999;6:54–68.
3. De Puey EG, Rozanski A. Using gated technetium-99m sestamibi SPECT to characterize fixed myocardial defects as infarct or artifact. *J Nucl Med.* 1995;36:952–955.
4. Mas J, Younes B, Bidet R. Improvement of quantification in SPECT studies by scatter and attenuation compensation. *Eur J Nucl Med.* 1989;15:351–356.
5. Hutton BF, Osiecki A, Meikle SR. Transmission-based scatter correction of 180 degrees myocardial single-photon emission tomographic studies. *Eur J Nucl Med.* 1996;23:1300–1308.
6. El Fakhri G, Buvat I, Benali H, Todd-Pokropek A, Di Paola R. Relative impact of scatter, collimator response, attenuation, and finite spatial resolution corrections in cardiac SPECT. *J Nucl Med.* 2000;41:1400–1408.
7. Links JM, Becker LC, Rigo P, et al. Combined corrections for attenuation, depth-dependent blur and motion in cardiac SPECT: a multicenter trial. *J Nucl Cardiol.* 2000;7:414–425.
8. Almquist H, Arheden H, Arvidsson AH, Pahlm O, Palmer J. Clinical implication of down-scatter in attenuation-corrected myocardial SPECT. *J Nucl Cardiol.* 1999;6:406–411.
9. Folks RD, Garcia EV, Cullom SJ, Case JA, Galt JR, Bateman TM. Reduction of gender differences in attenuation corrected stress Tc-99m myocardial perfusion SPECT normal databases [abstract]. *J Nucl Med.* 2001;42(suppl):4P.
10. Links JM, De Puey EG, Taillefer R, et al. Relative roles of gating and attenuation correction in improving accuracy of myocardial perfusion SPECT [abstract]. *J Nucl Med.* 2001;42(suppl):4P.
11. Goerres GW, Heidelberg TH, Schwitter MR, Burger C, Berthold T, Von Schulthess GK. Respiratory movement and accuracy of PET-CT fusion in the thorax [abstract]. *J Nucl Med.* 2001;42(suppl):12P.
12. Lee Z, Kemper CA, Muzic RF, Berridge MS, Wilson DL. Quantitative pulmonary imaging based on PET-CT co-registration with warping [abstract]. *J Nucl Med.* 2001;42(suppl):10P.
13. Wackers FJT. Attenuation correction, or the emperor's new clothes? *J Nucl Med.* 1999;40:1310–1312.
14. Prvulovich EM, Lonn AHR, Bomanji JB, Jarritt PH, Ell PJ. Effect of attenuation correction on myocardial thallium-201 distribution in patients with a low likelihood of coronary artery disease. *Eur J Nucl Med.* 1997;24:266–275.
15. Holland AE, Goldfarb JW, Edelman RR. Diaphragmatic and cardiac motion during suspended breathing: preliminary experience and implications for breath-hold MR imaging. *Radiology.* 1998;209:483–489.
16. Pitman AG, Kalf V, Van Every B, Risa B, Barnden LR, Kelly MJ. On the origins of the respiratory artefact species: effect of breathing patterns [abstract]. In: Program and abstracts of the Australian and New Zealand Society of Nuclear Medicine 2001 Annual Scientific Meeting; May 18–22, 2001; Hobart, Tasmania, Australia. Abstract 47:65.
17. Matsunari I, Boning G, Ziegler SI, et al. Effects of misalignment between transmission and emission scans on attenuation corrected cardiac SPECT. *J Nucl Med.* 1998;39:411–416.
18. Eisner R, Churchwell A, Noever T, et al. Quantitative analysis of the tomographic thallium-201 myocardial bullseye display: critical role of correcting for patient motion. *J Nucl Med.* 1988;29:91–97.
19. Cooper JA, Neumann PH, McCandless BK. Effect of patient motion on tomographic myocardial perfusion imaging. *J Nucl Med.* 1992;33:1571–1573.
20. Prigent FM, Hyun M, Berman DS, Rozanski A. Effect of motion on thallium-201 SPECT studies: a simulation and clinical study. *J Nucl Med.* 1993;34:1845–1850.
21. Lee DS, So Y, Cheon GJ, et al. Limited incremental diagnostic values of attenuation noncorrected gating and ungated attenuation correction to rest/stress myocardial perfusion SPECT in patients with an intermediate likelihood of coronary artery disease. *J Nucl Med.* 2000;41:852–859.
22. Vidal R, Buvat I, Darcourt J, et al. Impact of attenuation correction by simultaneous emission/transmission tomography on visual assessment of <sup>201</sup>Tl myocardial perfusion images. *J Nucl Med.* 1999;40:1301–1309.
23. Harel F, Genin R, Daou D, et al. Clinical impact of combination of scatter, attenuation correction and depth dependent resolution recovery for Tl-201 studies [abstract]. *J Nucl Med.* 2001;42(suppl):4P.

24. Ficaro EP, Fessler JA, Shreve PD, Kritzman JN, Rose PA, Corbett JR. Simultaneous transmission/emission myocardial perfusion tomography: diagnostic accuracy of attenuation corrected Tc-99m sestamibi single photon emission tomography. *Circulation*. 1996;93:463-473.
25. Gallowitsch HJ, Sykora J, Mikosch P, et al. Attenuation corrected thallium-201 single photon emission tomography using a gadolinium-153 moving line source: clinical value and the impact of attenuation correction on the extent and severity of perfusion abnormalities. *Eur J Nucl Med*. 1998;25:220-228.
26. Chouraqui P, Livschitz S, Sharir T, et al. Evaluation of an attenuation correction method for thallium-201 myocardial perfusion tomographic imaging of patients with low likelihood of coronary artery disease. *J Nucl Cardiol*. 1998;5:369-377.
27. Kluge R, Sattler B, Seese A, Knapp W. Attenuation correction by simultaneous emission-transmission myocardial single-photon emission tomography using a technetium-99m labelled radiotracer: impact on diagnostic accuracy. *Eur J Nucl Med*. 1997;24:1107-1114.
28. Gordon D, Pettway V, Links J, Mixon L, Anstett FG. Evaluation of equivalence of transmission attenuation corrected and prone myocardial perfusion imaging [abstract]. *J Nucl Med*. 2001;42(suppl):4P.
29. Cho K, Kumiata S, Okada S, Kumazaki T. Development of respiratory gated myocardial SPECT system. *J Nucl Cardiol*. 1999;6:20-28.

